Journal of The
Electrochemical Society

The Effect of Surface Pretreatment of Aluminum Alloy 7075-T6 on the Subsequent Inhibition by Cerium(III) Acetate in Chloride-Containing Solution

To cite this article: Ingrid Milošev and Peter Rodič 2022 *J. Electrochem. Soc.* **169** 011504

Journal of The Electrochemical Society, 2022 **169** 011504

The Effect of Surface Pretreatment of Aluminum Alloy 7075-T6 on the Subsequent Inhibition by Cerium(III) Acetate in Chloride-Containing Solution

Ingrid Milošev[*,z] **and Peter Rodič**

Jožef Stefan Institute, Department of Physical and Organic Chemistry, Jamova c. 39, SI-1000 Ljubljana, Slovenia

The study aimed to investigate the effect of surface pretreatment on the corrosion protection of aluminum alloy 7075-T6 in sodium chloride solution using cerium acetate as a corrosion inhibitor. Different surface pretreatments were tested: (i) mechanical grinding, (ii) mechanical grinding and non-water diamond polishing, (iii) mechanical grinding, alkaline etching with NaOH and acid desmutting, and (iv) mechanical grinding, alkaline cleaning with a commercial SurTec cleaner and acid desmutting. Topography, composition, and morphology of inhibited surface during immersion were investigated using optical microscopy, 3-D profilometry, scanning electron microscopy/energy-dispersive X-ray analysis and Fourier transform infrared spectrometry. The corrosion properties were determined by potentiodynamic measurements and electrochemical impedance spectroscopy in sodium chloride solution without and with the addition of cerium acetate. A change in the composition and morphology of the inhibited surface was noticed as a function of surface pretreatment and immersion time. Appropriate surface treatment resulted in improved protection against localized corrosion even after long-term immersion up to 1 month. Among mechanical pretreatments, polishing gave better results than grinding. Among chemical pretreatments, alkaline cleaning in SurTec/HNO_3 was more appropriate as a preceding step to acid desmutting than alkaline etching with NaOH.

 [DOI: 10.1149/1945-7111/ac4933]

Manuscript submitted November 10, 2021; revised manuscript received January 4, 2022. Published January 19, 2022. *This paper is part of the JES Focus Issue on Women in Electrochemistry.*

Supplementary material for this article is available online

Aluminum alloy (AA) 7075-T6 is suitable for versatile applications in the aircraft and automobile industry due to its excellent mechanical properties. This alloy is heat-treatable with zinc, magnesium and copper as major alloying elements,[1] which are present mainly as intermetallic particles (IMPs) within the alloy structure. Due to the IMPs, the alloy surface is electrochemically diverse, i.e. IMPs can be less noble (corrosion potential more negative relative to the matrix, e.g. for Al-Cu-Mg-Zn) or more noble (corrosion potential more positive relative to the matrix, e.g. for Al-Fe-Cu-Mn-Zn) relative to the matrix.[2] In the presence of aggressive chloride ions, the alloy is subject to localized corrosion processes such as galvanic, pitting and intergranular corrosion which usually start at the IMP sites. Eventually, these processes reduce the strength and stability of the alloy.[3]

Improving the corrosion resistance of aluminum alloy under service conditions is a key issue for successful applications. For decades this role has been played by chromate conversion coatings that assure good corrosion protection and have the ability of self-repair.[4] Since 2017, chromate coatings have been banned or restricted.[5] Among contemporary, environmentally friendly coatings, those based on rare-earth salts are being widely investigated.[6–9] The most effective rare-earth compounds are cerium(III) salts where the inhibition effect is based on the precipitation of $Ce(OH)_3$ at more noble IMPs at the surface.[9–14] This process occurs due to a local increase in pH during reduction reaction at the cathodic IMP sites. Cerium ions react with hydroxide ions and form $Ce(OH)_3$. In neutral solutions simultaneously existing $Ce(OH)_3$ and $Ce(OH)_2^{2+}$ can be slowly transformed to CeO_2.[a] Therefore, both Ce(III) and Ce(IV) species are responsible for inhibiting the alloy surface.[15,16] Arnott et al. showed that longer exposure times (20 d) of AA7075 resulted in the formation of 140 nm thick cerium oxide coating throughout the surface.[17] Our previous work reported that different cerium compounds, namely nitrate, chloride and acetate, exhibit different inhibition efficiency in sodium chloride solution on AA7075-T6 and AA2024-T3 alloys.[14–16,18,19] Diphenyl phosphate[20–22] and mercaptoacetate[23] were also studied as Ce compounds because the type of anion of the cerium compounds also affects the course of the inhibition mechanism. Among chloride salts, praseodymium and lanthanum were also reported as efficient corrosion inhibitors; therefore, the type of cation is important as well.[24] Temperature also affects the degree of protection: at temperatures above 50 °C, the inhibition becomes limited due to the increased corrosion rate of AA2024-T3 and slow pH establishment on the surface.[25,26]

Grinding, polishing and/or chemical treatment are common steps for surface preparation of metals in a laboratory and industrial practice. Grinding and polishing are standard mechanical treatments to remove oxide film entirely and produce a uniform surface with a native oxide film. On the other hand, the chemical treatment includes surface cleaning, degreasing, alkaline etching, and desmutting, where native oxide layer removal and the surface composition are better controlled.[27–29] In more detail, alkaline activation of 7075-T6 at pH > 11.5 causes thickening of the surface oxide to about ~20–60 nm, mainly consisting of magnesium-rich oxide. Degreasing removes ~20 nm of magnesium-rich oxide.[27] During alkaline cleaning, the aluminum-rich surface oxide is dissolved into the solution due to the formation of $Al(OH)_4^-$.[27,30] Cleaning is usually followed by acid desmutting aiming to remove residues of alkaline cleaning, to form the oxide film and to increase surface roughness to facilitate the adhesion of the coating on the surface. The type of surface pretreatment strongly affects the morphology and composition of the surface of AA7075-T6 and AA2024-T3.[9,31,32] In magnesium-containing aluminum alloys, water polishing may induce the preferential dissolution of magnesium; therefore, non-water polishing is the potential option for producing a more uniform surface.[9,31]

The protection by cerium salts can be achieved in a non-accelerated manner (i.e. by direct immersion of the solution of cerium salt with or without sodium chloride solution) or by an accelerated manner by adding hydrogen peroxide.[14–16,18,19,33–35] Direct immersion of the ground AA6061-T6%-10%Al_2O_3 sample in 1000 ppm $CeCl_3$ solution resulted in non-uniform deposition of Ce oxides; in contrast, the surface subject to pickling in KOH, boiling in distilled water and immersion in the same $CeCl_3$ solution produced a thick oxide with Ce deposited within pores in the oxide.[36] Ce-based conversion coatings deposited

*Electrochemical Society Member.
[z]E-mail: ingrid.milosev@ijs.si
[a]$Ce(OH)_3 + OH^- \rightarrow CeO_2 + 2H_2O$ and $Ce(OH)_2^{2+} + 2OH^- \rightarrow CeO_2 + 2H_2O$.

from $CeCl_3$ in the presence of H_2O_2 expressed better corrosion protection after alkaline activation AA7075-T6 substrates in Na_2CO_3 than in NaOH; the surface had fewer surface cracks and craters and was more uniform than that activated with NaOH.[37] Coatings prepared in a bath containing $CeCl_3$ at 40 °C with H_2O_2 accelerator provided the optimal corrosion protection when the AA7075-T6 substrate was alkaline etched in NaOH and cleaned in H_2SO_4.[38] In contrast, Ce coatings prepared in a bath containing $CeCl_3$ at 50 °C with H_2O_2 accelerator provided the optimal corrosion protection when the AA2024-T3 and AA7075-T6 substrates were alkaline cleaned by commercial cleaners and not desmutted in acid.[34,35] The described literature data show that the effect of surface pretreatment is complex and dependent on the type of alloy, composition and pH of cleaning and etching agents, temperature, type of cerium treatment, etc. Similar effects were also shown for other types of conversion coatings. i.e. trivalent chromium process (TCP)[39–41] and Zr- and Ti-based coatings.[42,43]

The AA7075-T6 has low corrosion resistance in NaCl solution because this alloy is prone to galvanic corrosion, pitting corrosion, stress corrosion cracking, crevice corrosion and dealloying even after a few hours of immersion.[15,18,19,31] Our previous studies dealt with: (i) the morphology, composition, wettability and corrosion properties of the AA7075-T6 after various mechanical and chemical pretreatments,[31] and (ii) various Ce(III) salts as corrosion inhibitors of mechanically ground AA7075-T6.[14–16,18,19] The focus of this study was the correlation between various surface pretreatments before and after immersion in sodium chloride with added Ce(III) acetate shown previously to be the most effective inhibitor when added to sodium chloride.[14–16,18,19] The main hypothesis is that even more effective inhibition can be achieved using an appropriate surface pretreatment, creating the surface properties stimulating the deposition of Ce-oxide. Non-accelerated conditions without H_2O_2 were used, as in our previous publications.[14–16,18,19] The surface pretreatment and cerium film formation were analyzed in terms of composition, topography, morphology and electrochemical properties, also during long-term testing (up to 1 month).

Experimental

Materials and chemicals.—Substrate and pretreatments.—The bare AA7075-T6, 2 cm × 4 cm sized specimens, cut from 0.5 mm thick flat sheets, distributed by Kaiser Aluminum, USA, were used as substrate. The nominal composition of alloy given in weight percentage (wt. %) is 5.81% Zn, 2.55% Mg, 1.67% Cu, 0.21% Fe, 0.08% Si and the remainder Al.

The samples were subject to four mechanical and chemical pretreatments:

a) grinding with 2400 and 4000-grit SiC emery papers (Struers, Denmark) using a grinding machine (Struers LaboPol-5, Denmark) at a rotation speed of 300 rms in the presence of tap water,
b) grinding as described in a) followed by non-water polishing using 1 μm diamond paste and alcohol-based lubricant,
c) grinding as described in a) followed by chemical pretreatment,[31] by immersion in 0.01 M NaOH (pH = 11.6) for 3 min followed by desmutting in 50% HNO_3 (pH = 1.5) for 3 min at room temperature (denoted as NaOH/HNO_3) and
d) grinding as described in a) followed by commercial chemical treatment[31] by immersion in a mixture of 3 wt. % SurTec132 and 0.5 wt. % SurTec089 (pH = 8.3) for 3 min at 40 °C followed by desmutting in 50% HNO_3 (pH = 1.5) for 3 min at room temperature (denoted as SurTec/HNO_3).

After mechanical and chemical pretreatment, the sample was rinsed thoroughly with deionized water (Milli Q Direct water, resistivity greater than 18.2 MΩ·cm at 25 °C and a total organic carbon (TOC) value below 5 ppb, Millipore, Billerica, MA, USA), cleaned ultrasonically in pure ethanol (absolute ⩾99.8%, Sigma-Aldrich) for 10 min and finally dried with a stream of pure compressed nitrogen.

Chemicals and solutions.—Polishing was performed using the polishing machine (Struers LaboPol-5, Denmark) at rotation speed 300 rms together with a polishing cloth (MD/DP-Nap cloth), diamond paste 1 μm (DP-paste P) and ethanol-based lubricant (DP-Lubricant Blue), all supplied by Struers. The chemicals used for chemical surface treatments were: NaOH (ApplicaChem, 99%, Germany), HNO_3 (Sigma Aldrich, 66%, Germany), SurTec132 liquid recyclable builder and SurTec089 recyclable detergent (SurTec, Germany).

Immersion tests and electrochemical measurements were performed in 0.1 M NaCl, pH = 5.5 (AppliChem, > 99.5%, Germany). The cerium(III) acetate ($Ce(OAc)_3$: $Ce(CH_3COO)_3 \times 2H_2O$, 99.9%, Sigma-Aldrich, Germany) was added at the concentration of 3 mM, which was proved as optimal concentration.[18,19] Determination of crystal-bound water in $Ce(OAc)_3$ was calculated from the thermogravimetric analysis. Cerium oxide CeO_2 (99.9%, Sigma-Aldrich, Germany) and $Ce(OAc)_3$ powders were used as reference materials in FTIR analysis.

The addition of $Ce(OAc)_3$ changes the pH of the 0.1 M NaCl solution from pH = 5.5 to pH = 6.8. All solutions were prepared using Milli-Q Direct water.

Methods.—Immersion test.—Immersion testing of the corrosion resistance after various surface pretreatment was performed by immersion in 0.1 M NaCl solution containing 3 mM $Ce(OAc)_3$ in 100 ml polyethylene vials open to air at room temperature. The test lasted up to one month, but the samples were tested after selected immersion times (before, after 3 d and 1 month) to follow the progress of the corrosion/inhibition with time. After the immersion test, the samples were rinsed with deionised Milli Q water and dried with a stream of compressed nitrogen. The test was carried out in triplicate for each immersion time/surface pretreatment; the surface analyses presented below were performed on the same representative sample.

Surface analysis.—The surface appearance of AA7075-T6 during the immersion test was analyzed using a digital optical camera and a confocal microscope (Axio, CDM 700, Zeiss, Gottingen, Germany) with 20× objective zoom.

The topography of sample surface after different surface treatments was characterized with contact profilometer DektakXT, Brucker, Germany, using Vision64 software. At least three repetitions at different points in the center of the sample were performed and the representative measurement was chosen. The measured surface area was 1 mm × 1 mm. The radius of the needle was 2 μm and the force of the needle on the alloy surface was 1 mg. Surface parameters, i.e. mean surface roughness (S_a) and 3D profiles, were obtained using TalyMap Gold 6.2 (Taylor-Hobson, Leicester, UK) software data processing.

A field-emission scanning electron microscope (SEM) (Jeol JSM-7600F) was used to image the surface's morphology. Before the analysis, a few nm thick carbon layer was deposited onto the coating surface. SEM analysis was performed with a voltage of 2 and 5 kV using three different modes: compositional contrast (COMPO), low secondary electron image (LEI) and secondary electron image (SE). Energy-dispersive X-ray spectroscopy (EDS) analyses were performed with a voltage of 15 kV.

The chemical composition of the surface was analyzed using universal attenuated total reflectance Fourier transform infrared spectroscopy (ATR FTIR) (PerkinElmer Spectrum). The spectra were measured in the range from 4000 to 500 cm^{-1}, with a resolution of 4 cm^{-1}, by averaging four scans. All spectra are presented as transmittance.

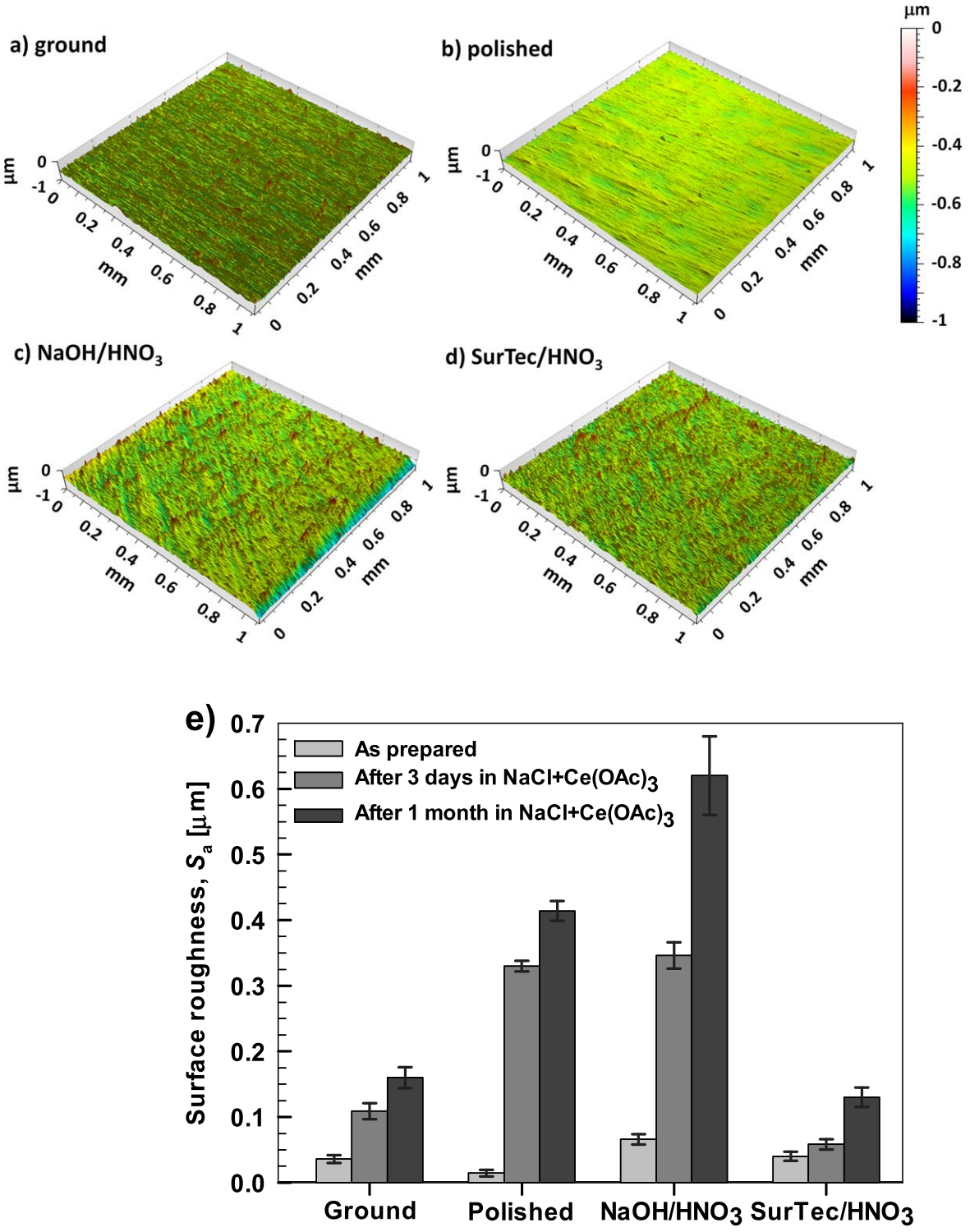

Figure 1. 3-D side profiles of the AA7075-T6 samples subject to different surface treatments: (a) ground, (b) ground and polished, and ground and chemically treated with (c) $NaOH/HNO_3$ and (d) $SurTec/HNO_3$. The coloring is according to the scale on the right, which spans the 1 μm range. The image spot size was 1 mm × 1 mm. Figure (e) shows the estimated surface roughness (S_a) before (as prepared) and after immersion in the $NaCl+Ce(OAc)_3$ solutions for 3 d and 1 month.

Electrochemical measurements.—Electrochemical measurements were performed in a three-electrode standard corrosion cell (Parstat, Corrosion Cell Kit, model K0047, volume 1 L) at 25 ± 2 °C. Substrate disks embedded in a Teflon holder (model K0105 Flat Specimen Holder Kit), leaving an area of 0.95 cm^2 exposed to the corroding solution, served as a working electrode. A saturated calomel electrode (SCE, 0.242 V vs saturated hydrogen electrode) placed in a Luggin capillary salt bridge was used as a reference electrode. A carbon rod served as a counter electrode. Electrochemical experiments were carried out with an Autolab PGSTAT 12 (Metrohm Autolab, Utrecht, The Netherlands) potentiostat/galvanostat equipped with a frequency response analyzer

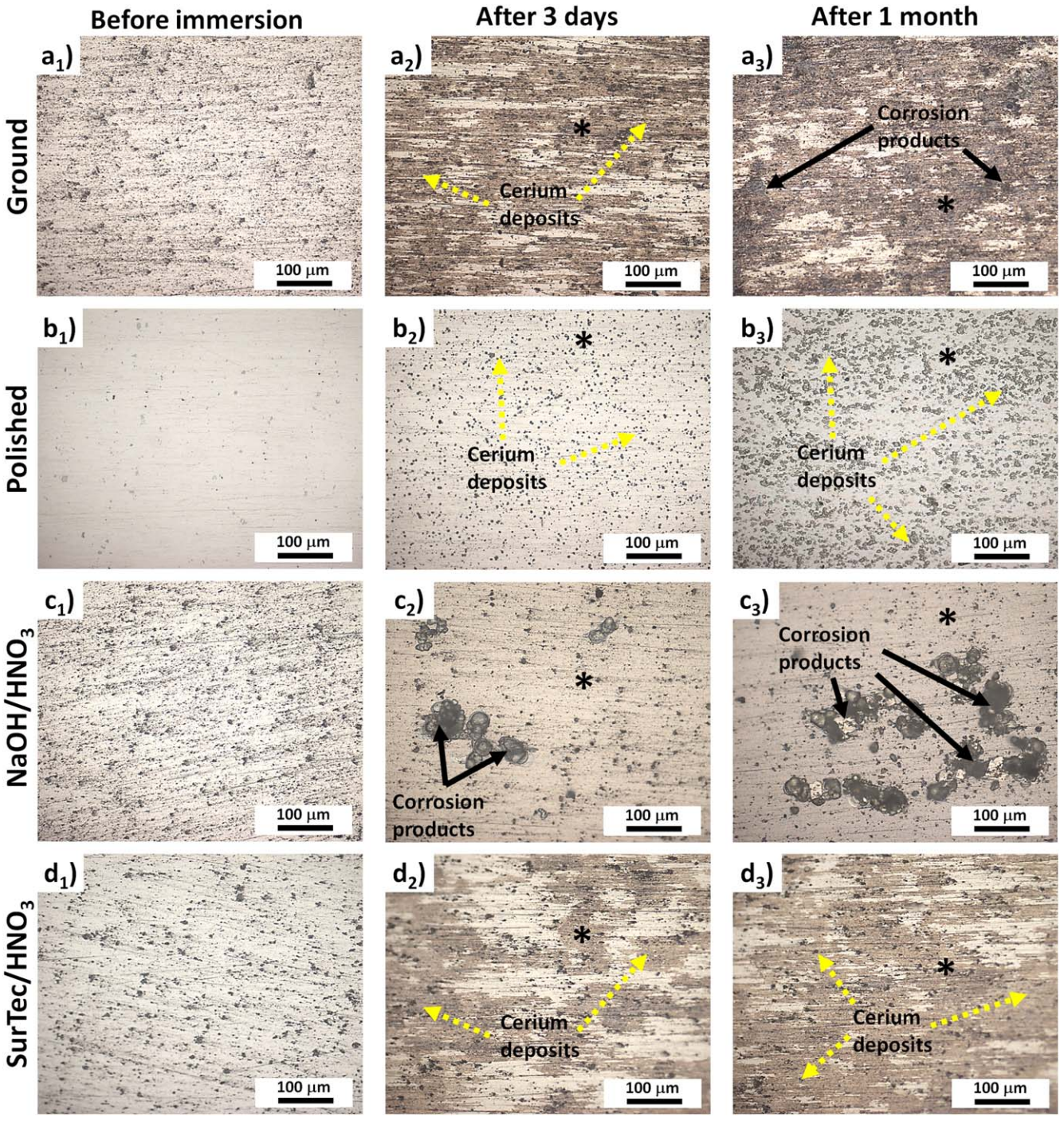

Figure 2. Confocal images of the surface appearance of the AA7075-T6 samples subject to different surface treatments: (a) ground, (b) ground and polished, and ground and chemically treated with (c) $NaOH/HNO_3$ and (d) $SurTec/HNO_3$ before and after immersion in the $NaCl+Ce(OAc)_3$ solutions for 3 d and for 1 month. Black solid arrows mark the corrosion products on the alloy surface. Dashed yellow arrows mark the cerium deposits on the alloy surface. Comparative SEM images are presented in Fig. 3. Further, for samples in each vertical column, SEM images at high magnification are given in Fig. 4 (before immersion, i.e. as prepared), Fig. S2 (after 3 d of immersion) and Fig. 5 (after 1 month of immersion). The asterisks mark the positions where the SEM analyses were performed.

module for electrochemical impedance measurements and controlled by Nova 2.1 software.

Electrochemical potentiodynamic measurements.—Before the measurements, the samples were allowed to stabilize under open-circuit conditions for 1 h. The stable, quasi-steady state potential reached at the end of the stabilization period is denoted as the open circuit potential (E_{oc}). Following stabilization, potentiodynamic measurements were performed using a 1 mV s^{-1} scan rate, starting at –250 mV to E_{oc}. The potential was then increased in the anodic direction. For each sample, measurements were performed in at least triplicate. The most representative measurement (at least two replicates) was chosen for plotting and determination of electrochemical parameters: corrosion current density (i_{corr}), corrosion potential (E_{corr}), pitting potential (E_{pit}) and the difference $\Delta E = |E_{corr} - E_{pit}|$. E_{corr} and i_{corr} were evaluated by Tafel approximation, and E_{pit} was determined as an intersection of the straight lines through the passive region and the abrupt increase in the current density. ΔE denotes the span of the passive region. It should be emphasized that some polarization curves with not well-defined

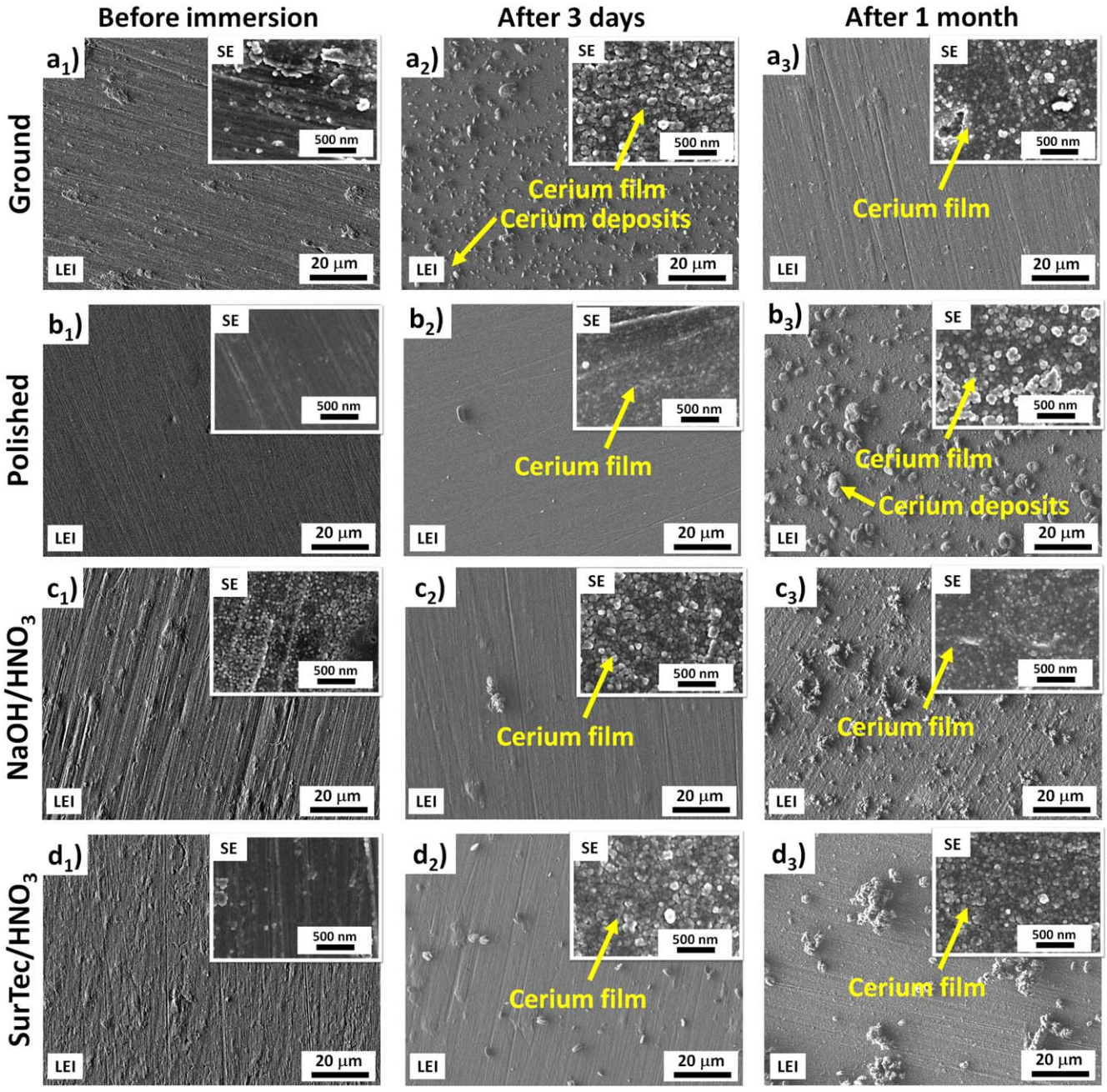

Figure 3. SEM LEI and SE images of the AA7075-T6 samples subject to different surface treatments: (a) ground, (b) ground and polished, and ground and chemically treated with (c) $NaOH/HNO_3$ and (d) $SurTec/HNO_3$ before and after immersion in the $NaCl+Ce(OAc)_3$ solutions for 3 d and for 1 month.

anodic Tafel regions were extrapolated by inspecting only a linear fit of the cathodic Tafel curve, which intersects the E_{corr}.

Electrochemical impedance spectroscopy.—The corrosion behavior during long-term immersion was monitored using electrochemical impedance spectroscopy (EIS). The frequency range was from 100 kHz to 10 mHz at a sinusoidal voltage amplitude of 10 mV (rms). The sample was immersed in 0.1 M NaCl solution with or without the addition of 3 mM $Ce(OAc)_3$ at 25 ± 2 °C. The EIS spectra were recorded at the open circuit potential at selected time intervals up to 1 month.

Results and Discussion

Topography, morphology and composition.— *Pretreated samples.*—Pretreated AA7075-T6 samples were first analyzed as-prepared. The topography of samples subject to various surface treatments of the aluminum alloy surface was analyzed by a 3D profilometer (Figs. 1a–1d). The grinding produces a rough surface with a mean roughness S_a = 0.036 μm because the scratches remained on the surface despite using fine abrasive papers with small SiC powder (Fig. 1e). The hardness of IMPs present in the alloy differs from the aluminum matrix; therefore, they can be torn. After polishing with 1 μm diamond paste in the presence of non-water lubricant, the roughness was reduced to S_a = 0.015 μm. Chemical pretreatment using $NaOH/HNO_3$ resulted in increased roughness (S_a of 0.066 μm) compared to the ground surface that can be explained by selective etching of the passive film and intermetallics present on the aluminum surface in alkaline media and desmutting of etched residuals from the surface. Chemical treatment using $SurTec/HNO_3$ produced S_a of 0.040 μm. The surface pretreatment with $SurTec/HNO_3$ is well-controlled, resulting in a slight difference

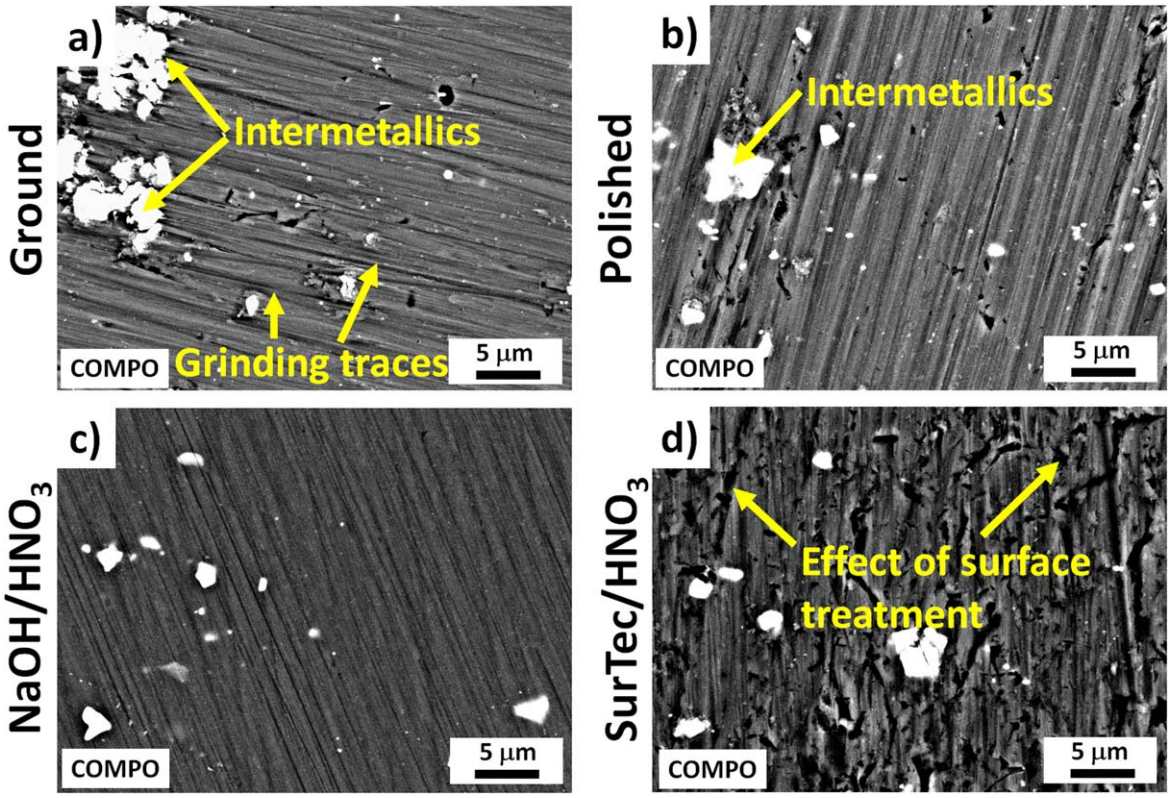

Figure 4. SEM COMPO images of the AA7075-T6 samples subject to different surface treatments: (a) ground, (b) ground and polished, and ground and chemically treated with (c) $NaOH/HNO_3$ and (d) $SurTec/HNO_3$.

Table I. Results of the EDS analyses performed on the numbered spots in SEM images of AA7075-T6 after grinding, grinding and polishing, and grinding and chemical treatments in $NaOH/HNO_3$ and $SurTec/HNO_3$. After pretreatment, samples were immersed in the 0.1 M NaCl + 3 mM $Ce(OAc)_3$ for one month (SEM images presented in Fig. S2 and Fig. 5).

		Atomic percentage (at.%)					
Numbered spots	Pretreatment	Al	O	Zn	Mg	Cu	Ce
1	Ground	84.5	9.1	2.7	2.5	0.9	0.3
2	Polished	69.0	22.4	1.9	1.7	0.6	4.4
3	$NaOH/HNO_3$	81.9	11.5	2.8	2.3	1.2	0.3
4	$SurTec/HNO_3$	77.8	16.1	2.4	2.2	0.9	0.6

in surface roughness compared to the ground surface and a more homogeneous surface.

Figures S1 (available online at stacks.iop.org/JES/169/011504/mmedia) (optical images at lower magnification), Fig. 2 (confocal images) and Fig. 3 (SEM images in LEI and SE modes) show the appearance and morphology of AA7075-T6 after various surface pretreatments before (as prepared) and after 3 d and 1 month of immersion in NaCl+$Ce(OAc)_3$. First, we will consider the effect of surface pretreatment on the as-prepared samples (left vertical columns in Figs. S1, 2 and 3 denoted with subscript 1: a_1, b_1, c_1, d_1). The difference in the surface appearance was noticed between ground, and ground and polished mechanically pre-treated samples (Figs. S1a_1 and b_1 and Figs. 2a_1 and b_1). The grinding process removed the naturally formed oxide film, but many scratches remained on the surface. Moreover, secondary phases, i.e. IMPs of various shapes and sizes, are noticed (Figs. 2a_1 and b_1), especially for the sample ground under water. This is more clearly visible in high magnification SEM images in Figs. 3a_1 and Fig. 4a. The AA7075-T6 has a heterogeneous structure with many micrometre-sized randomly spread IMPs. Ground alloy surface exhibited some surface defects; on the other hand, the polished sample surface was smoother (Figs. 2b_1, 3b_1 and 4b). The difference in the mechanical treatment affects the surface composition (a native oxide layer formed by self-passivation and composition of alloying elements in the IMPs).[31] Further, mechanical treatment can create an altered surface layer on Al alloys that has been shown to influence corrosion properties.[44–46] In contrast, the fine polishing using diamond paste minimized the defects and produced a more uniform surface with significantly fewer scratches. The IMPs remained homogeneously spread in the aluminum matrix (Fig. 4b). Thus, polishing in water-free lubricant is a much softer procedure than grinding under water and is also more reproducible. This is noticed in the LEI images in Fig. 3b_1 with the polished surface exhibiting a uniform morphology down to nanometric level (inset), whereas the ground surface is rather non-uniform, showing various surface features at the nanometric level (inset in Fig. 3a_1).

In the next set, we compared the effect of chemical treatment using NaOH (pH = 11.6) or SurTec (pH = 8.3) followed by desmutting in HNO_3 (Figs. S1c_1 and S1d_1 and Figs. 2c_1 and 2d_1). The general appearance of the chemically pre-treated surface is rougher compared to mechanically pre-treated ones (Fig. 1). SEM images in LEI mode are presented in Figs. 3c_1 and 3d_1. After

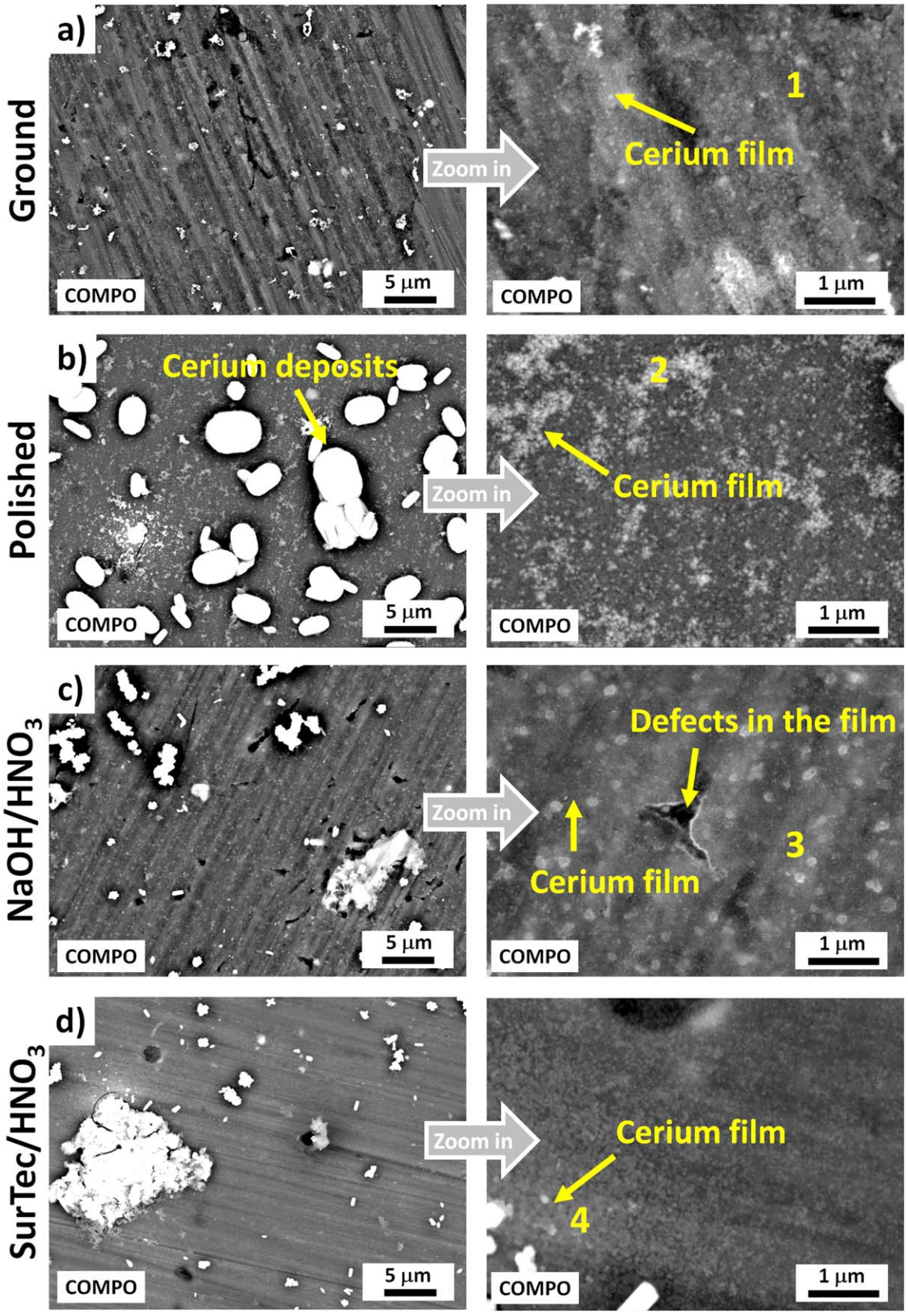

Figure 5. SEM COMPO images of the AA7075-T6 samples subject to different surface treatments: (a) ground, (b) ground and polished, and ground and chemically treated with (c) $NaOH/HNO_3$ and (d) $SurTec/HNO_3$ and immersed in 0.1 M NaCl containing 3 mM $Ce(OAc)_3$ for 1 month. The numbered spots present the positions where the EDS analysis were performed (Table I).

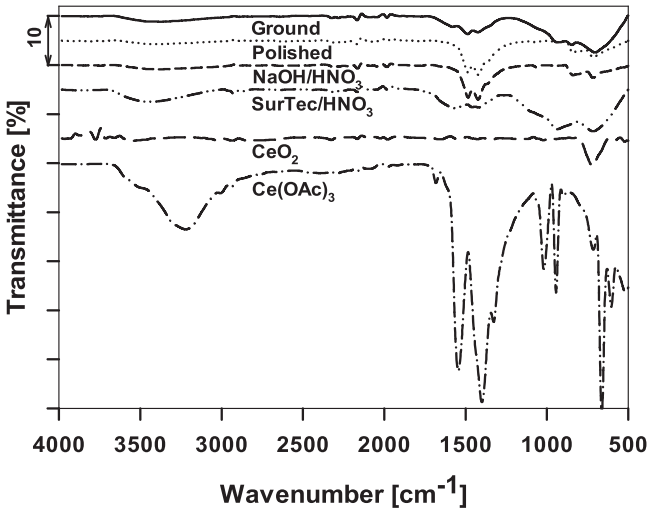

Figure 6. ATR FTIR spectra of AA7075-T6 samples subject to different surface treatments: ground, ground and polished, and ground and chemically treated with $NaOH/HNO_3$ and $SurTec/HNO_3$ after immersion in 0.1 M NaCl containing 3 mM $Ce(OAc)_3$ for 3 d. Additionally, the spectra for reference compounds CeO_2 and $Ce(OAc)_3$ are added as a benchmark. Spectra taken after 1-month immersion are given in Fig. S4.

$SurTec/HNO_3$ pretreatment (Fig. $3d_1$), the surface is at the nanometric level more similar to those after the mechanical treatments (insets in Figs. $3a_1$ and $3b_1$). After $NaOH/HNO_3$ pretreatment, a thicker surface film was formed (Fig. $3c_1$). The shape and distribution of IMPs after chemical treatment is generally more similar to that after grinding but IMPs are less spread and torn out (Fig. 4). Chemical pretreatments did not remove the grinding marks and larger surface defects caused by the mechanical treatment remained.

The chemical pretreatment changes the chemical composition of the surface film because it removes the oxide film and selectively dissolves the metals present in the intermetallics, as shown in our previous study.[31] $NaOH/HNO_3$ treatment results in the enrichment of the surface with Zn and spongy, Cu-rich remnants and reduced Mg content since Mg-hydroxide, formed in NaOH, is dissolved in acidic pH.[31] SurTec/NaOH pretreatment does not produce enrichment in Cu remnants.[31]

Pretreated samples immersed in sodium chloride solution with added Ce(III) acetate.—The S_a values evaluated from 3D images are depicted in Fig. 1e. For all samples, S_a increased with immersion time in $NaCl+Ce(OAc)_3$ due to the formation of the cerium-acetate rich layer at the surface. However, the difference between initial and final roughness is strongly dependent on the pretreatment. It is the largest for $NaOH/HNO_3$ and polished samples and the smallest for $SurTecH/HNO_3$ sample. The surface roughness increased significantly due to the formation of cerium deposits on the alloy surface, as will be shown by subsequent SEM/EDS analysis.

Now we will consider the changes of the surface topography, morphology and composition in the course of immersion of differently pre-treated samples immersed in $NaCl+Ce(OAc)_3$ for 3 d (middle vertical columns in Figs. S1, 2 and 3 denoted with subscript 2: a_2, b_2, c_2, d_2) and 1 month in $NaCl+Ce(OAc)_3$ (right vertical columns in Figs. S1, 2 and 3 denoted with subscript 3: a_3, b_3, c_3, d_3). After 3 d of immersion, surface film formation was noticed on the ground alloy surface (Fig. $S1a_2$ and Fig. $2a_2$). The cerium film was not formed uniformly on the whole surface but in some areas. This is better observed in SEM images recorded in LEI and SE modes (Fig. $3a_2$) and COMPO mode (Fig. S2a). For the latter, insoluble cerium oxide particles formed on the surface of ground AA7075-T6 after 3 d of immersion are visible as bright spots. The inhibition mechanism of cerium salts like nitrate and chloride proceeds by precipitation of cerium hydroxide at more noble IMPs.[7,10–12,14] In contrast, the addition of cerium acetate results in the precipitation of cerium oxide particles not only at the IMPs but also on the surrounding aluminum oxide matrix.[14,18,19] The enlarged image indeed shows that the particles are rice-like shaped and approximately 800 nm in length (Fig. S2a). These particles, identified as cerium oxide,[19] are present throughout the surface and also at the IMPs (denoted as light grey spots within the matrix). After extended immersion of 1 month in $NaCl+Ce(OAc)_3$, the cerium film was present but still did not cover the surface evenly (Figs. $S1a_3$, $2a_3$, $3a_3$ and 5a). The identification of cerium in the surface film is evidenced by the EDS analysis given in Table I (the analysis sites are denoted in Fig. 5).[b] However, it should be noted that at some spots at the surface the localized corrosion of different types of IMPs was noticed (Fig. $2a_3$). Localized corrosion was described in detail previously[19] and ascribed to the preferential dissolution of Mg-rich particles leaving behind Cu-rich particles, and the dissolution of the matrix around primarily noble Al-Cu-Fe-Mn particles leading to so-called trenching.[19]

The formation of cerium film on a polished surface differs from that on the ground surface (Figs. S1b and 2b). No corrosion damage was noticed during immersion, indicating that $Ce(OAc)_3$ effectively inhibited the corrosion of AA7075-T6 for up to one month. Cerium film covers the whole surface, as clearly observed in the COMPO image in Fig. S2b and related EDS analysis in Fig. 5b and Table I, as well as by SE images at high magnification showing precipitated particles of up to a few micrometers (Figs. $3b_2$ and $3b_3$). The increased number of deposits formed after the prolonged immersion of one month on the polished surface compared to that on the ground surface correlates well with the observed change in topography (Fig. 1e).

The crucial difference in surface pretreatments was reflected in the formation of cerium film on the chemically treated surface (Figs. S1c and S1d and Figs. 2c and 2d). The $NaOH/HNO_3$ pretreatment had a negative impact on the formation of cerium film and consequently on the inhibition efficiency of $Ce(OAc)_3$. After 3 d of immersion, a large part of the sample was covered with corrosion products, confirming that the added cerium compound cannot efficiently protect the surface against corrosion (Figs. $S1c_2$ and $2c_2$). After 1 month, the thick layer of corrosion products covered almost the whole alloy surface (Figs. $S1c_3$ and $2c_3$). At sites where no corrosion products were formed, the cerium precipitation took place (Figs. $3c_3$ and S2c) but that was insufficient to protect the surface from corroding. The length of precipitated particles was up to 3−4 μm. EDS analysis confirmed the formation of Ce film (Table I) although SEM images at higher magnification (Fig. 5c) show that some defects in the film were formed.

The chemical pretreatment with $SurTec/HNO_3$ enhances a more uniform formation of cerium films over the whole surface and no corrosion products were observed (Figs. S1d, 2d and 3d). The Ce-containing surface layer (Fig. 5d, Table I) seems compact and was formed on the whole surface. It seems that this layer is most uniform and dense among differently pre-treated samples. High magnification SEM COMPO image and related EDS spectra confirm an abundant formation of Ce-deposits (Fig. S3).

As already noted, the surface roughness of the alloy surface is affected by chemical pretreatment (Fig. 1e). After presenting SEM images and EDS results we can now state that the large increase in S_a for $NaOH/HNO_3$ pre-treated surface can be explained by a non-uniform cerium deposition on alloy surface and some corrosion products (up to 0.346 μm after 3 d and 0.620 μm after 1 month). A similar trend is observed on the polished surface. On the other hand, the surface roughness of alloy pre-treated with $SurTec/HNO_3$ was not changed significantly, confirming more evenly formed cerium film on the whole surface (S_a was 0.058 μm after 3 d and 0.130 μm after one month).

[b] After 3 d of immersion Ce was not detected by EDS. This was due to the high voltage used for analysis (15 kV); therefore, results are not given in the table; however, that does not mean that the Ce film was not present after 3 days since it was clearly observed by SEM (Fig. S2).

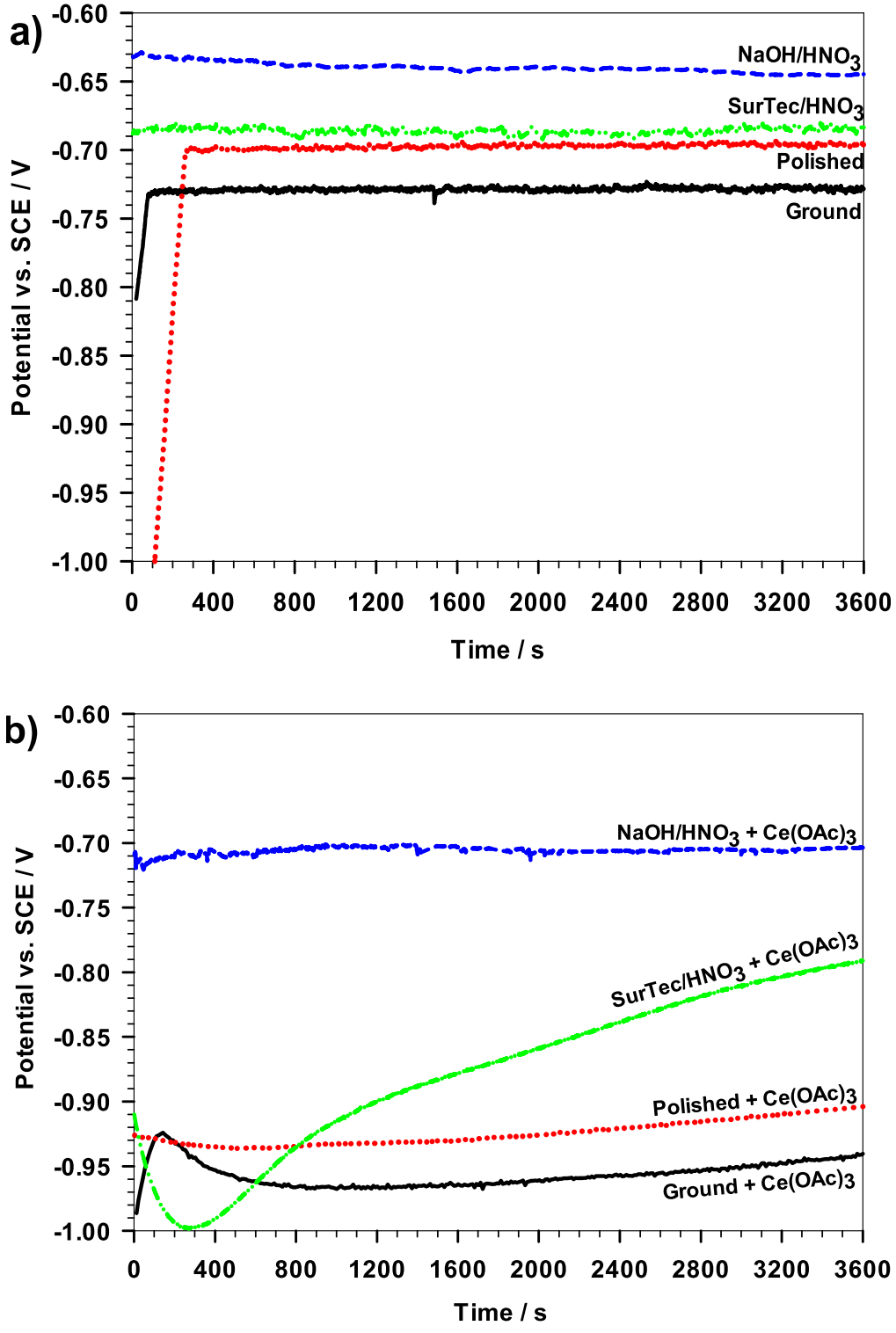

Figure 7. The open circuit potential as a function of immersion time measured in (a) 0.1 M NaCl and (b) 0.1 M NaCl containing 3 mM $Ce(OAc)_3$ for AA7075-T6 samples subject to different surface treatments: ground, ground and polished, and ground and chemically treated with $NaOH/HNO_3$ and $SurTec/HNO_3$.

The cerium oxide is formed at the matrix and on IMPs (Fig. 5, S2 and S3, Table I). The atomic percentage of cerium is between 0.3–0.6, as shown by EDS. Uniform and dense layer is formed without any cracks for ground, polished and $SurTec/HNO_3$ pre-treated surface. The FTIR spectroscopy was used to identify further the functional groups of the product formed at the AA7075–T6 surface during immersion in $NaCl+Ce(OAc)_3$. Cerium(III) acetate, $Ce(OAc)_3 \times 2H_2O$, was analyzed as a reference compound (Fig. 6). It shows characteristic bands at 3204, 2982, 1683, 1544, 1399, 1352, 1052, 945, 666, and 609 cm^{-1}. The bands between 1500 and 1330 cm^{-1} in metal acetates [47–49] have been assigned to asymmetric and symmetric COO^- stretching vibrations. The position of the bands depends on the type of metal.[47,48] In particular, for cerium acetate, these bands were reported at 1539 and 1451 cm^{-1}.[47] The

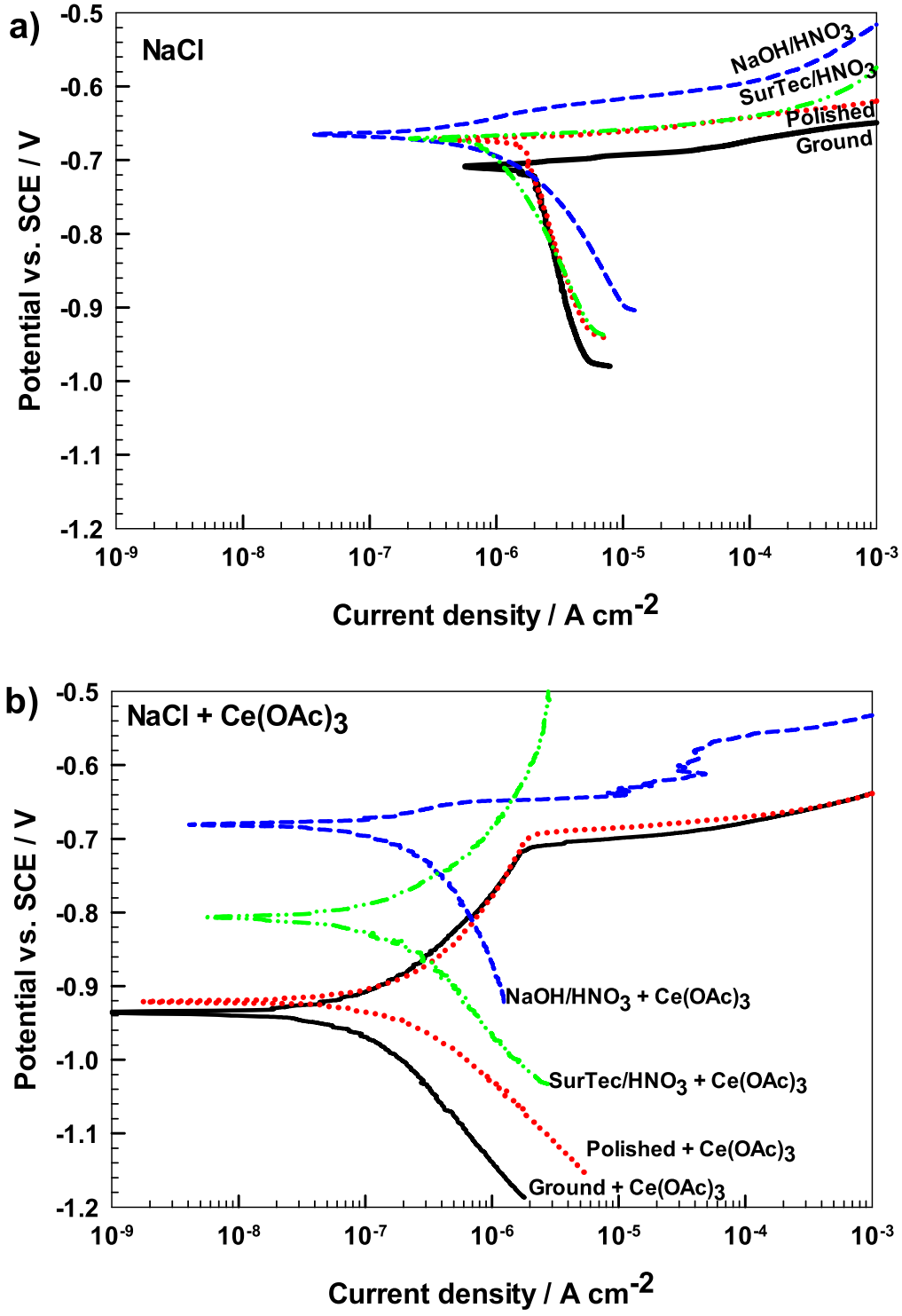

Figure 8. Potentiodynamic polarization curves measured in (a) 0.1 M NaCl and (b) 0.1 M NaCl containing 3 mM $Ce(OAc)_3$ for AA7075-T6 samples subject to different surface treatments: ground, ground and polished, and ground and chemically treated with $NaOH/HNO_3$ and $SurTec/HNO_3$. $dE/dt = 1$ mV s^{-1}. The curves were recorded after 1 h stabilization at the E_{oc}. Figure 7. Electrochemical parameters are given in Table II.

absorption bands between 521 and 848 cm^{-1} are related to cerium, i.e. Ce−O stretching vibrations.[48,50] The absorption bands at 3319, 2138 and 1642 cm^{-1} correspond to physically adsorbed water molecules. The adsorption bands between 2000 and 3000 cm^{-1} are assigned to OH stretching vibrations of H_2O in the sample.

FTIR spectra were recorded at the surface of AA7075-T6 surface after immersion in 0.1 M NaCl containing 3 mM $Ce(OAc)_3$ for 3 d (Fig. 6) and one month (Fig. S4). The low intensity of the FTIR bands after 3 d indicates that only a thin layer of inhibitor coating was formed, which does not give an intense ATR FTIR spectrum. The spectra indicate the presence of cerium compound at the surface, showing strong bands at 1490, 1479, 1362, 1052, 858, 724, 712, 698 and 667 cm^{-1}. Bands characteristic of carboxylate can be recognized, confirming the formation of layer originating from $Ce(OAc)_3$. A small shift observed in comparison to reference $Ce(OAc)_3$ powder can be due to the bonding of the Ce compound to the aluminum alloy

Table II. Electrochemical parameters after grinding, grinding and polishing, and grinding and chemical treatments using NaOH/HNO_3 and SurTec/HNO_3 were measured for AA7075-T6 in 0.1 M NaCl without or with the addition of 3 mM of cerium acetate. i_{corr} (corrosion current density), E_{corr} (corrosion potential), E_{pit} (pitting potential) and the span $\Delta E = |E_{corr} - E_{pit}|$ were determined from potentiodynamic polarization curves (Fig. 8).

	Electrochemical parameters			
Pretreatment	i_{corr} [μA cm^{-2}]	E_{corr} [V]	E_{pit} [V]	ΔE [mV]
	NaCl			
Ground[a)]	1.86	–0.70	–0.69	10
Polished	1.51	–0.67	–0.66	10
NaOH/HNO_3	0.19	–0.63	–0.62	10
SurTec/HNO_3	0.85	–0.68	–0.67	10
	NaCl + Ce(OAc)$_3$			
Ground[a)]	0.062	–0.94	–0.71	230
Polished	0.085	–0.92	–0.69	230
NaOH/HNO_3	0.055	–0.68	–0.65	30
SurTec/HNO_3	0.061	–0.81	/	> 250

a) Data already published in Ref. 18.

surface. The spectrum contains additional sharp bands at 858 cm^{-1} and several bands in the range between 724 and 667 cm^{-1}, which can be ascribed to Ce−O stretching vibrations.[48]

Upon longer immersion (1 month) in the $Ce(OAc)_3$ inhibitor solution, the composition of the inhibited layer at the surface remained similar (Fig. S4) because the main difference is in the band intensity low wavenumbers (between 500 and 1200 cm^{-1}). These bands do not coincide with those of the carboxylic group typical for acetate compound, indicating that another type of cerium compound is formed in the course of prolonged immersion. This compound does not correspond entirely to the reference cerium(IV) oxide powder, CeO_2, which shows characteristic bands at 717 cm^{-1} (Fig. S4). The comparative spectra for the Ce(III) oxide could not be taken due to the insolubility of this oxide. It is known that the inhibition by cerium(III) salt results in the formation of a mixed Ce (III) and Ce(IV) oxide/hydroxide.[14,16,51] We assume that the product formed upon prolonged immersion corresponds to such oxide/hydroxide compound of mixed (III)/(IV) valence.[15,16,51] The inhibition mechanism may proceed in two phases as a function of time: in the first phase cerium acetate-rich compound is formed, which over time gradually transform into a cerium oxide-rich compound.

Electrochemical properties and corrosion protection.—Potentiodynamic measurements in sodium chloride solution.— The effects of mechanical and chemical surface pretreatments on the electrochemical characteristics were first studied in 0.1 M NaCl solution. Time dependence of E_{oc} values of AA7075-T6 samples subject to different pretreatments is presented in Fig. 7a. For both chemically treated samples, E_{oc} was stabilized immediately upon immersion and was more positive compared to that of mechanically treated samples. This is related to the presence of the oxide film that is formed by chemical treatment and desmutting.[31] The oxide layer formed on NaOH/HNO_3 contains Zn and Cu remnants, whereas that on SurTec/HNO_3 contains less Zn, no Cu enrichment but also Si and P originating from chemical degreasing agent. In contrast, mechanically treated samples initially show more negative potentials that within 300 s reached a quasi-steady value. As mentioned above, the mechanical treatment created a thin altered surface layer (ASL) that has a different microstructure than the underlying bulk substrate (so-called "Beilby" layer). Wang et al. have shown that the ASL layer formed on AA7075-T6 makes the surface more susceptible to corrosion due to the formation of Zn-rich nano-grains[46] but that formed on AA2024-T3 can be less susceptible to corrosion than the bulk alloy.[52] Our previous study showed that the AA7075 surface, polished under non-aqueous condition, contained more Mg and Zn than ground surface[31]; the presence of these less noble elements lead to more negative E_{oc}. After ~300 s, the quasi-steady E_{oc} is established for all samples with values between −0.64 V and −0.73 V. Small fluctuations of potential are still observed, reflecting the occurrence of constant corrosion process even on the stabilized sample.

The effect of surface treatment is also reflected in polarization curves (Fig. 8a). Electrochemical parameters deduced from polarization curves are presented in Table II. In the cathodic region, the oxygen reduction reaction proceeds primarily at the IMPs, which are electrochemically more noble compared to the surrounding alloy matrix covered by native oxide. The cathodic current densities were similar for ground, polished and SurTec/HNO_3 samples and somewhat larger for NaOH/HNO_3. Compared to the ground sample, E_{corr} of other samples shifted to more noble values up to 30 mV. These surface treatments thus reduce the kinetics of corrosion by reducing the cathodic current density, probably due to the formation of the aluminum oxide-based layer over surfaces containing IMPs, thus leading to limitation of access of oxygen for the reduction reaction. All samples showed an abrupt increase in current density at $E > E_{corr}$ (ΔE within 10 mV) due to fast initiation of localized corrosion on AA7075-T6 in chloride medium. For the NaOH/HNO_3 sample, a slightly slower increase was observed.

The observed effect on electrochemical response is the consequence of composition and morphological changes of the surface caused by different treatments (Figs. 2–5). Grinding and polishing result in the thinning of the native oxide layer, but the IMPs have been shown to retain more magnesium with polishing than with grinding under water.[31] The presence of electrochemically active Mg at the surface may induce the shift of E_{corr} to a more active region. Further, polishing with the diamond paste can cause severe plastic strain to the surface especially near and on the intermetallic components and promote localized corrosion along grain boundaries.[53] The polished sample exhibited somewhat smaller i_{corr} values but still of the same order of magnitude as the ground sample (Table II). For the NaOH/HNO_3 and SurTec/HNO_3 samples the i_{corr} is reduced, reaching down to one order of magnitude smaller values compared to ground and polished samples (Table II). The pH of 0.01 M NaOH is almost 12 (pH = 11.6), i.e., at the verge of the stability of magnesium-rich oxide $Mg(OH)_2$ and verge of instability of aluminum oxide where it dissolves as aluminate ions $Al(OH)_4^-$. Therefore, etching with NaOH results in the formation of the Mg-rich layer.[27,31] During the subsequent desmutting step, Mg is dissolved and Al-oxide is re-formed. Its formation may cause some degree of protection of the surface, as observed in the anodic part (Fig. 8a). The solution of the SurTec cleaning agent is milder (pH = 8.3). It consists of tetrapotassium pyrophosphate, which can react with the alloy, as phosphate was identified at the surface.[31] pH is lower than that at which the formation of Mg-oxide would be formed.

Potentiodynamic measurements in sodium chloride solution with added cerium acetate.—The effect of the surface treatments on the time dependence of E_{oc} of AA7075-T6 also in 0.1 M NaCl solution containing cerium acetate is shown in Fig. 7b. The initial E_{oc} values of ground, polished and SurTec/HNO_3 samples were shifted more negative for about 250 mV in the presence of $Ce(OAc)_3$ (between −0.81 V and −0.93 V) compared to uninhibited NaCl solution. The curves changed with immersion time: the curve for the ground sample remained most negative followed by that of the polished sample. For SurTec/HNO_3 sample the curve showed an initial drop and then a gradual shift in a positive direction. This behavior may be related to the initial activation of the surface and subsequent development of the inhibited layer. As will be shown in Fig. 8b, this surface pretreatment provided the best performance in inhibited solution. In contrast, For NaOH/HNO_3 sample showed the most positive E_{oc} (−0.70 V), which was only slightly changed compared to that in uninhibited solution. This behavior indicates that this

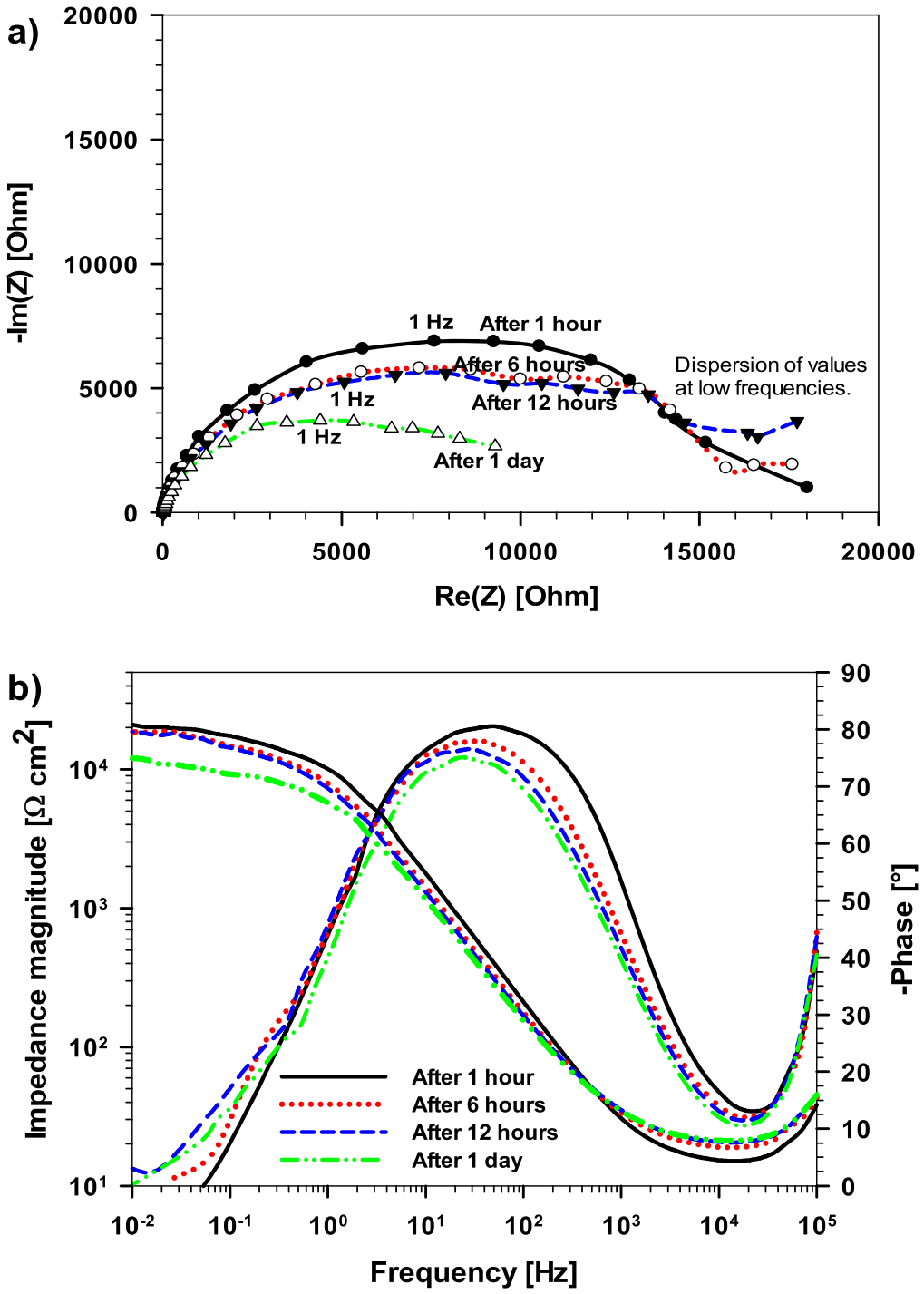

Figure 9. (a) Nyquist plots and (b) Bode plots of magnitude of impedance and phase angle recorded in 0.1 M NaCl for ground AA7075-T6. Spectra were recorded after different immersion times up to 1 d.

chemical pretreatment produces a surface that is less prone to inhibition with cerium.

Related potentiodynamic polarization curves and deduced electrochemical parameters are presented in Fig. 8b and Table II. The cathodic current densities are largely reduced in 0.1 M NaCl containing $Ce(OAc)_3$ compared to the uninhibited solution (Fig. 8a), down to two orders of magnitude, indicating the suppressed reaction of oxygen reduction (Fig. 8b). The position of E_{corr} reflects the differences observed under open-circuit conditions, i.e., the most negative shift was obtained for ground and polished sample, and the smallest for $NaOH/HNO_3$.

Ground, polished and $NaOH/HNO_3$-treated samples showed E_{pit} similar as in an uninhibited solution. However, for the former two samples, E_{corr} shifted in the negative direction resulting in ΔE of more than 200 mV (Table II). The increase of the current density above E_{corr} was slower as well. For the $NaOH/HNO_3$-treated sample, E_{corr} remained similar as in uninhibited solution and, consequently, no broadening of ΔE was observed. The anodic current density increased almost immediately following E_{corr}. The $SurTec/HNO_3$-treated sample showed E_{corr} at about -0.8 V, i.e.130 mV more negative than in uninhibited solution, but no pitting was observed in the measured region.

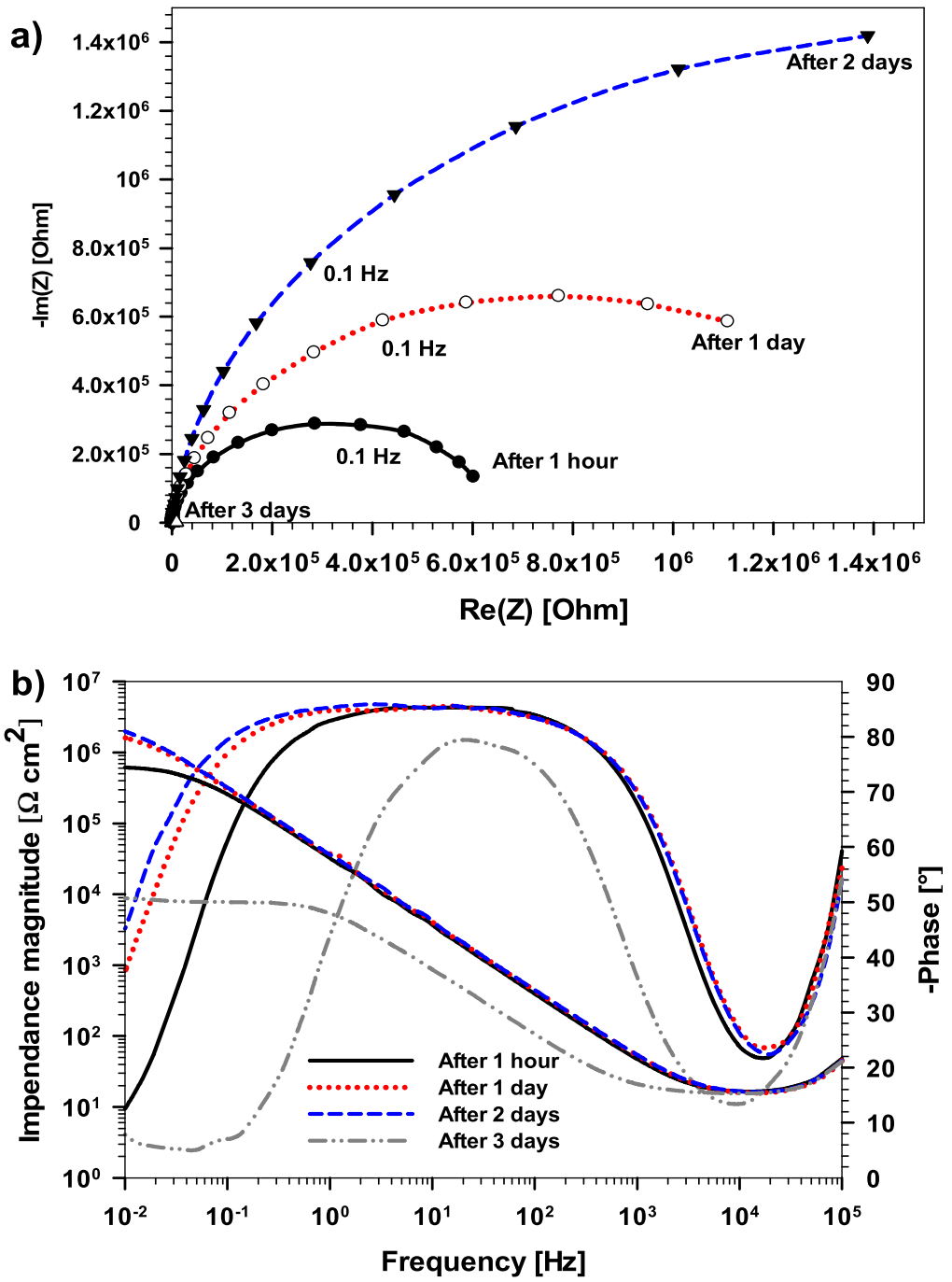

Figure 10. (a) Nyquist plots and (b) Bode plots of magnitude of impedance and phase angle recorded in 0.1 M NaCl containing 3 mM $Ce(OAc)_3$ for ground AA7075-T6. Spectra were recorded after different immersion times up to 3 d.

Based on the presented potentiodynamic results, i.e. shape of the curves and electrochemical parameters, we can state that mechanical treatments and chemical treatment using SurTec/HNO_3 were more appropriate than chemical treatment using NaOH/HNO_3 due to its narrow ΔE and higher susceptibility to pitting corrosion of the latter treatment. SEM analysis already showed that the grinding as well as NaOH/HNO_3 are not the optimal pretreatments as both samples showed evidence of corrosion damage after 1 month of immersion (Fig. 2 and S1). Nonetheless, we performed long-term EIS measurements to complement the results of the immersion test and related SEM/EDS analysis.

Long-term electrochemical impedance spectroscopy in sodium chloride solution with added cerium acetate.—EIS spectra in the form of Nyquist plots and Bode plots of magnitude of impedance and phase angle are presented for AA7075-T6 immersed in NaCl (Fig. 9) and NaCl containing $Ce(OAc)_3$ (Figs. 10, 11, S5 and S6). In uninhibited NaCl, the shape of EIS spectra is typical for the development of pitting corrosion of aluminum alloy.[54] Spectra were taken after 1 h, 6 h, 12 h and 1 d. The common feature of the Nyquist plots is a single semicircle; its diameter reflects the relaxation time constant of the charge-transfer resistance, approximately equal to the diameter. At low frequency, a dispersion is observed, related to the appearance of pitting corrosion already at the early stage of immersion (Fig. 9a). The diameter of the semi-circle decreased with immersion time. In Bode plots where three distinct regions are observed: the high-frequency region where the phase angle approaches 0°, as is typical for resistive behavior, the middle

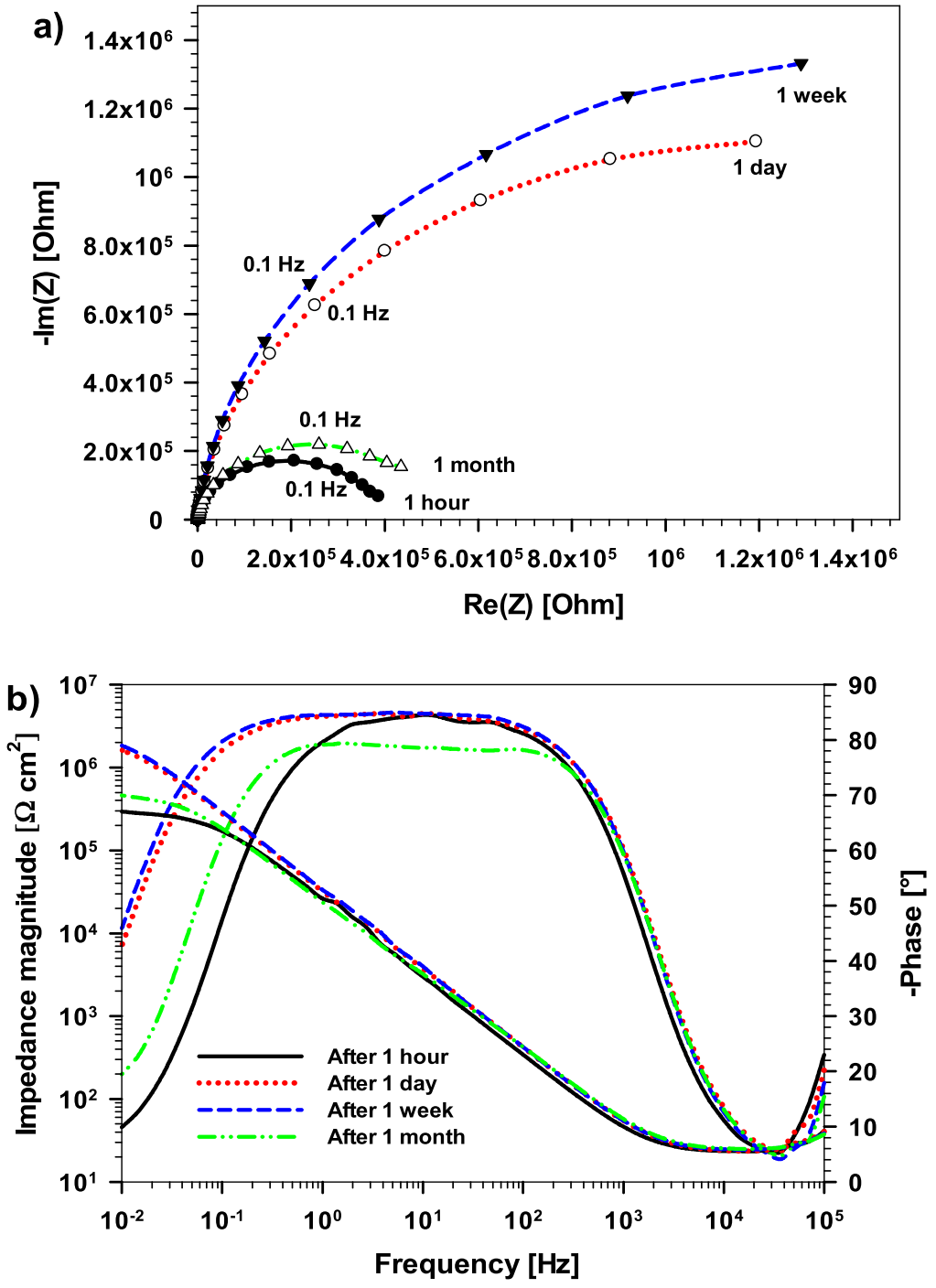

Figure 11. (a) Nyquist plots and (b) Bode plots of magnitude of impedance and phase angle recorded in 0.1 M NaCl containing 3 mM $Ce(OAc)_3$ for ground AA7075-T6 chemically treated with SurTec and desmutted in HNO_3. Spectra were recorded after different immersion times up to 1 month.

frequency where the impedance increases linearly with frequency as it decreases (Fig. 9b). The plateau is reached at approximately $10^4\ \Omega\ cm^2$ and a phase angle of $-80°$. A transmission line type at the intermediate frequencies can be related to the development of pitting corrosion.[54] At lower frequencies, the phase angle decreased. These changes in shapes of the curve with increasing immersion time suggest that chloride ions initiate and promote the development of pitting on AA7075-T6. After one day pitting was evident.

The inhibited ground alloy exhibits a completely different EIS response (Fig. 10). The diameter of the capacitance loop increased with increasing time during the initial few hours. It was one order of magnitude larger than in an uninhibited solution. The diameter of the semi-circle increased up to two days. The change is evident in Bode plots as increased linear part of the magnitude of impedance plot at intermediate frequencies related to the capacitive nature of the surface layer, the increased impedance at low frequencies and a broader range of frequencies at which the phase angle is constant. After three days, however, the impedance was reduced (Fig. S7).

EIS spectra for the inhibited polished sample are given in Fig. S5. The shape of the curves is similar to those of ground alloy in $NaOH+Ce(OAc)_3$ but the protection was prolonged. Namely, the impedance magnitude and phase angle remained high for more than one week, which is significantly longer compared to the inhibited ground sample with values decreasing after 2 d (Fig. 10).

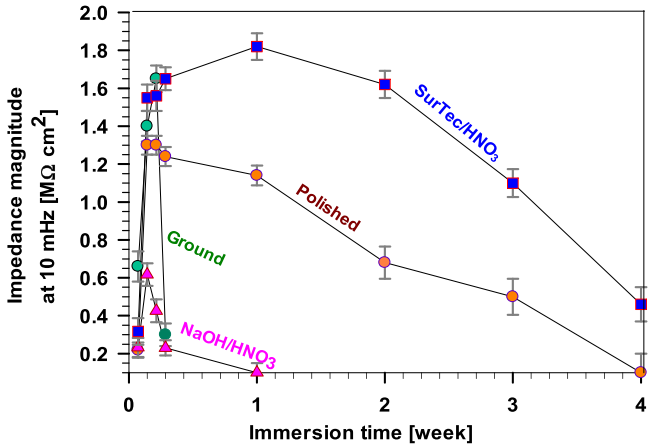

Figure 12. Impedance magnitude at 10 mHz $|Z_{10\ mHz}|$ as a function of immersion time in 0.1 M NaCl containing 3 mM $Ce(OAc)_3$ up to 4 weeks measured for the AA7075-T6 samples subject to different surface treatments: ground, ground and polished, and ground and chemically treated with $NaOH/HNO_3$ and $SurTec/HNO_3$. The results are presented as the mean value ± standard deviation.

When the sample chemically treated in $NaOH/HNO_3$ was immersed in $NaOH+Ce(OAc)_3$ the EIS response reflected the formation of non-protective film and localized corrosion process (Fig. S6). In contrast, when the sample was pre-treated chemically using $SurTec/HNO_3$, the long-term protection in the presence of inhibitor was more efficient (Fig. 11). With increasing immersion time, the diameter of the semi-circle increased up to one week (Fig. 11a). Bode plots also reflect the significant improvement of corrosion resistance. After one month, the magnitude of impedance was reduced compared to 1-week immersion but it was still higher than after 1 h immersion (Fig. 11b). The low frequencies plateau at $\sim 10^6\ \Omega\ cm^2$ was three orders of magnitude larger than in uninhibited solution (Fig. 9). Bode plots of phase angle show a broad region of frequencies where the value is constant, indicating the stability of the inhibited substrate. These results suggest that cerium ions create efficient corrosion protection. The inhibition is relatively fast, observed already after one hour, and remained high for at least one week; afterwards, it decreased but still surpassed that in uninhibited solution.

The comparison of the EIS results for different surface pretreatment is presented as the impedance magnitude at 0.01 Hz ($|Z_{at\ 10\ mHz}|$) a function of immersion time in $NaCl+Ce(OAc)_3$ (Fig. 12). The $|Z_{at\ 10\ mHz}|$ for ground AA7075-T6 reached its maximum after 2 d (1.65 MΩ cm^2) and afterwards the impedance quickly decreased. On the other hand, the $|Z_{at\ 10\ mHz}|$ for the polished surface was somewhat lower, reaching its maximum (1.3 MΩ cm^2) after 3 d, but then decreased rather slowly (two-three weeks) to initial values thus reflecting more efficient corrosion inhibition compared to the ground sample (Figs. 3 and 5). Also, corrosion areas were readily observed on the ground sample immersed in $NaCl+Ce(OAc)_3$, where similar areas were very limited on polished samples (Fig. 2).

The lowest impedance was obtained for $NaOH/HNO_3$ pre-treated surface (Fig. 12). The $|Z_{at\ 10\ mHz}|$ values were relatively high (maximum of 0.62 MΩ cm^2) within the first 2 d, but then decreased rapidly, reflecting the corrosion process (Fig. 2d$_3$). The best performance was achieved when the alloy surface was pre-treated with $SurTec/HNO_3$. After one week, $|Z_{at\ 10\ mHz}|$ reached higher values than those for polished and, especially, ground samples. The inhibition remained stable for a longer period and then slowly decreased but remained above initial values (after 1 h). This confirmed more durable corrosion inhibition for this chemically pre-treated surface.

Conclusions

Aluminum alloy 7075-T6 is subject to corrosion in chloride solution. Proper selection of mechanical and chemical pretreatments of the alloy surface affects the susceptibility to corrosion upon immersion in chloride solution in the presence of cerium acetate as an inhibitor added directly to the solution.

Morphology, topography and composition of the samples change as a function of surface pretreatment and determine the degree of inhibition. Among mechanical pretreatments, polishing provides a better basis for the formation of the protective cerium oxide layer. Among chemical pretreatments, cleaning with commercial, phosphate-based, slightly alkaline SurTec cleaner followed by desmutting in nitric acid produced a highly protective surface containing cerium-acetate-rich oxide particles forming a dense, uniform layer covering the entire surface.

The important message of this study is that corrosion inhibition is not related only to the efficiency of the corrosion inhibitor itself, but it is also strongly related to surface pretreatment.

Acknowledgments

The financial support by Slovenian Research Agency is acknowledged (grants No. P2-0393 and P1-0134). The authors thank Prof. Barbara Malič for the access to the FTIR instrument (Centre of Excellence NAMASTE). The authors also acknowledge the Centre of Excellence in nanoscience and nanotechnology—Nanocentre, Ljubljana, Slovenia to access the scientific equipment (FIB-SEM/EDS). The authors acknowledge Barbara Kapun, BSc, for performing FIB-SEM/EDS analysis.

ORCID

Ingrid Milošev https://orcid.org/0000-0002-7633-9954
Peter Rodič https://orcid.org/0000-0001-8664-0129

References

1. J. R. Davis, *Corrosion of Aluminum and Aluminum Alloys* (The United States of America, Novelty, Ohio) p. 327 (1999), ASM International.
2. R. G. Buchheit, *J. Electrochem. Soc.*, **142**, 3994 (1995).
3. Q. Meng and G. S. Frankel, *J. Electrochem. Soc.*, **151**, B271 (2004).
4. M. W. Kendig and R. G. Buchheit, *Corrosion*, **59**, 379 (2003).
5. European Parliament and of the Council, Commission implementing decision of 19.7.2017 granting an authorisation for certain uses of chromium trioxide and dichromium tris(chromate) under Regulation (EC) No 1907/2006 of the European Parliament and of the Council (2017), https://ec.europa.eu/docsroom/documents/25201.
6. R. Twite and G. Bierwagen, *Prog. Org. Coat.*, **33**, 91 (1998).
7. M. Bethencourt, F. J. Botana, J. J. Calvino, M. Marcos, and M. A. Rodríguez-Chacón, *Corros. Sci.*, **40**, 1803 (1998).
8. O. Gharbi, S. Thomas, C. Smith, and N. Birbilis, *Npj Mater. Degrad.*, **12**, 1 (2018).
9. T. G. Harvey, *Corros. Eng. Sci. Technol.*, **48**, 248 (2013).
10. A. J. Aldykewicz, H. S. Isaacs, and A. J. Davenport, *J. Electrochem. Soc.*, **142**, 3342 (1995).
11. A. Aballe, M. Bethencourt, F. J. Botana, M. J. Cano, and M. Marcos, *Mater. Corros.*, **52**, 344 (2001).
12. M. A. Arenas, M. Bethencourt, F. J. Botana, J. de Damborenea, and M. Marcos, *Corros. Sci.*, **43**, 157 (2001).
13. M. A. Arenas, A. Conde, and J. J. de Damborenea, *Corros. Sci.*, **44**, 511 (2002).
14. P. Rodič, I. Milošev, M. Lekka, F. Andreatta, and L. Fedrizzi, *Electrochim. Acta*, **308**, 337 (2019).
15. P. Rodič and I. Milošev, *Corros. Sci.*, **149**, 108 (2019).
16. P. Rodič, M. Lekka, F. Andreatta, I. Milošev, and L. Fedrizzi, *Electrochim. Acta*, **370**, 137664 (2021).
17. D. R. Arnott, N. E. Ryan, B. R. W. Hinton, B. A. Sexton, and A. E. Hughes, *Appl. Surf. Sci.*, **22–23**, 236 (1985).
18. P. Rodič and I. Milošev, *J. Electrochem. Soc.*, **163**, C85 (2016).
19. I. Milošev and P. Rodič, *Corrosion*, **72**, 1021 (2016).
20. N. Birbilis, R. G. Buchheit, D. L. Ho, and M. Forsyth, *Electrochem. Solid-State Lett.*, **8**, C180 (2005).
21. J.-A. Hill, T. Markley, M. Forsyth, P. C. Howlett, and B. R. W. Hinton, *J. Alloys Compd.*, **509**, 1683 (2011).
22. D. Ho, N. Brack, J. Scully, T. Markley, M. Forsyth, and B. Hinton, *J. Electrochem. Soc.*, **153**, B392 (2006).
23. R. Catubig, A. E. Hughes, I. S. Cole, B. R. W. Hinton, and M. Forsyth, *Corros. Sci.*, **81**, 45 (2014).

24. J. Li, B. Hurley, and R. Buchheit, *J. Electrochem. Soc.*, **162**, C563 (2015).
25. J. Li, B. Hurley, and R. Buchheit, *J. Electrochem. Soc.*, **163**, C845 (2016).
26. J. Li, B. Hurley, and R. Buchheit, *Corrosion*, **72**, 1281 (2016).
27. S. Joshi, W. G. Fahrenholtz, and M. J. O'Keefe, *Appl. Surf. Sci.*, **257**, 1859 (2011).
28. K. J. H. Nelson, A. E. Hughes, R. J. Taylor, B. R. W. Hinton, L. Wilson, and M. Henderson, *Mater. Sci. Technol.*, **17**, 1211 (2001).
29. Y. Liu, M. A. Arenas, A. de Frutos, J. de Damborenea, A. Conde, P. Skeldon, G. E. Thompson, P. Bailey, and T. C. Q. Noakes, *Electrochim. Acta*, **53**, 4454 (2008).
30. S. Joshi, W. G. Fahrenholtz, and M. J. O'Keefe, *J. Electrochem. Soc.*, **158**, C296 (2011).
31. U. Tiringer, J. Kovač, and I. Milošev, *Corros. Sci.*, **119**, 46 (2017).
32. S.-Y. Chen, C.-Y. Huang, and C.-S. Lin, *Corros. Sci.*, **184**, 109354 (2021).
33. P. Rodič and I. Milošev, *Stud. UBB Chem.*, **65**, 227 (2020).
34. J. J. Alba-Galvín, L. González-Rovira, M. Bethencourt, F. J. Botana, and J. M. Sánchez-Amaya, *Metals*, **9**, 320 (2019).
35. J. J. Alba-Galvín, L. González-Rovira, F. J. Botana, M. Lekka, F. Andreatta, L. Fedrizzi, and M. Bethencourt, *Metals*, **11**, 930 (2021).
36. A. S. Hamdy and A. M. Beccaria, *J. Appl. Electrochem.*, **35**, 473 (2005).
37. S. Joshi, W. G. Fahrenholtz, and M. J. O'Keefe, *Surf. Coat. Technol.*, **205**, 4312 (2011).
38. I. Danaee, H. R. Zamanizadeh, M. Fallahi, and B. Lotfi, *Mater. Corros.*, **65**, 815 (2014).
39. L. Li, A. L. Desouza, and G. M. Swain, *J. Electrochem. Soc.*, **161**, C246 (2014).
40. J. Qi, A. Němcová, J. R. Walton, X. Zhou, P. Skeldon, and G. E. Thompson, *Thin Solid Films*, **616**, 270 (2016).
41. C. F. Glover, M. L. C. Lim, G. Post, M. Mayo, and J. R. Scully, *Corrosion*, **75**, 1513 (2019).
42. P. Zhou, Y. Liu, L. Liu, B. Yu, T. Zhang, and F. Wang, *Surf. Coat. Technol.*, **377**, 124904 (2019).
43. I. Milošev and G. S. Frankel, *J. Electrochem. Soc.*, **165**, C127 (2018).
44. Z. Zhao and G. S. Frankel, *Corros. Sci.*, **49**, 3089 (2007).
45. Z. Zhao and G. S. Frankel, *Corrosion*, **63**, 613 (2007).
46. S.-S. Wang, G. S. Frankel, J.-T. Jiang, J.-F. Chen, S.-L. Dai, and L. Zhen, *J. Electrochem. Soc.*, **160**, C493 (2013).
47. J. E. Tackett, *Appl. Spectrosc.*, **43**, 483 (1989).
48. I. Medhat, N. Abdallah, and K. Diaa Eldin, *Indian J. Pure Appl. Phys. IJPAP*, **43**, 911 (2005).
49. M. Forsyth, C. M. Forsyth, K. Wilson, T. Behrsing, and G. B. Deacon, *Corros. Sci.*, **44**, 2651 (2002).
50. K. K. Babitha, A. Sreedevi, K. P. Priyanka, B. Sabu, and T. Varghese, "Indian." *J. Pure Appl. Phys.*, **53**, 596 (2015).
51. I. Santana, A. Pepe, E. Jimenez-Pique, S. Pellice, I. Milošev, and S. Ceré, *Surf. Coat. Technol.*, **265**, 106 (2015).
52. S.-S. Wang, F. Yang, and G. S. Frankel, *J. Electrochem. Soc.*, **164**, C317 (2017).
53. Z. Zhao and G. S. Frankel, *Corros. Sci.*, **49**, 3064 (2007).
54. F. Mansfeld, S. Lin, S. Kim, and H. Shih, *Mater. Corros.*, **39**, 487 (1988).